Journal of Alloys and Compounds 649 (2015) 375–379

Contents lists available at ScienceDirect

Journal of Alloys and Compounds

journal homepage: http://www.elsevier.com/locate/jalcom

Far-infrared spectroscopy of $Zn_{1-x}Mn_xGeAs_2$ single crystals: Plasma damping influence on plasmon – Phonon interaction

N. Romcevic [a, *], M. Romcevic [a], W.D. Dobrowolski [b], L. Kilanski [b], M. Petrovic [a], J. Trajic [a], B. Hadzic [a], Z. Lazarevic [a], M. Gilic [a], J.L. Ristic-Djurovic [a], N. Paunovic [a], A. Reszka [b], B.J. Kowalski [b], I.V. Fedorchenko [c, d], S.F. Marenkin [c, d]

[a] Institute of Physics, University of Belgrade, Pregrevica 118, 11080 Belgrade, Serbia
[b] Institute of Physics, Polish Academy of Science, 02-668 Warsaw, Poland
[c] Kurnakov Institute of General and Inorganic Chemistry RAS, 119991 Moscow, Russia
[d] National Institute of Science and Technology, MISiS, Moscow, Russia

ARTICLE INFO

Article history:
Received 12 June 2015
Received in revised form
8 July 2015
Accepted 10 July 2015
Available online 13 July 2015

Keywords:
Semiconductors
Electron–phonon interactions
Light absorption and reflection

ABSTRACT

The interest in thorough description of $Zn_{1-x}Mn_xGeAs_2$ arises from its suitability for application in the field of non-linear optics. The room temperature far-infrared reflectivity spectra of single crystals $Zn_{1-x}Mn_xGeAs_2$, where $0 \leq x \leq 0.078$, were measured in the spectral range from 80 cm^{-1} to 500 cm^{-1}. The spectra were analyzed by fitting procedure using a dielectric function which includes interaction between a plasmon and two different phonons. The detected phonons are in excellent agreement with the theoretical predictions. The MnAs cluster phonons are detected, as well.

1. Introduction

Ternary semiconductors of the form II-IV-V_2 are crystal-chemicals that are electrical twins of semiconductors of the form III-V. Ordered replacement of the atom III in a semiconductor by the atoms II and IV in a ternary semiconductor causes doubling of the unit cell size in the direction of the *c*-axis and consequent reduction of symmetry from the cubic to the tetragonal. For example, a representative of this group of materials, $ZnGeAs_2$ with the twin semiconductor GaAs, crystallizes in the chalcopyrite structure.

A diluted magnetic semiconductor whose Curie temperature is as high as 300 K can be obtained by doping $ZnGeAs_2$ with Mn [1,2]. The non-linear optical coefficients of the resulting alloy, i.e., of $Zn_{1-x}Mn_xGeAs_2$, are large [3], and its direct energy gap corresponding to $T = 300$ K at the Γ point of the Brillouin zone is $E_g = 1.15$ eV [4]. Due to these characteristics, the described material is suitable for application in the non-linear optics; hence the interest for its other attributes.

The plasmons of free carriers and the longitudinal-optical (LO) phonons interact through their macroscopic electric fields, and the result is appearance of the coupled LO phonon-plasmon modes (CPPMs). The vast majority of published studies are devoted to the *n*-type semiconductors and the interaction of a single phonon with effective plasmons. The studies involving the influence of the plasmon damping on the CPPM followed somewhat later [5]. For example, for low damping rates in the *n*-type GaAs, the coupled modes can be classified in an upper L_+ branch and a lower L_- branch. With the increase in the carrier density, i.e., plasma frequency, the nature of the upper mode changes in energy from the LO phonon-like to a plasmon-like. The change in the lower frequency mode occurs the other way around, reaching the transverse-optical (TO) phonon energy for large plasmon energy. The distinction between the upper and lower mode becomes meaningless for large plasmon dumping. In this case, one mode is more phonon-like with energy ω_{LO} for $\omega_P = 0$ and ω_{TO} for $\omega_P >> \omega_{LO}$, with nearly pure phonon damping in both cases, whereas the other mode is an overdamped plasmon mode. Further, it is the plasma with high mobilities and low effective masses of the carriers that is often considered, in which case is enabled the detection of low, L_-, and high, L_+, energy branch of the CPPM [6,7].

Despite the early theoretical prediction of the interaction between two phonons and a plasmon [8], experimental confirmations are rare [9–11]. As for the influence of the plasmon damping on the

* Corresponding author.
E-mail address: romcevi@ipb.ac.rs (N. Romcevic).

http://dx.doi.org/10.1016/j.jallcom.2015.07.087
0925-8388/

interaction between a plasmon and two different phonons, i.e. on the coupled plasmon-two-phonons modes, CP2PM, to the best of our knowledge it has not been considered so far.

Our intention is to use far-infrared spectroscopy to study the fundamental properties of the coupled plasmon-two-phonons modes in the *p*-type materials, as well as to further investigate these coupled modes under different plasmon damping conditions. The Raman spectra measurements performed on the $Zn_{1-x}Mn_xGeAs_2$ system [12] offer additional justification for the intended course of research.

2. Experimental technique, methods, and groundwork

The studied samples of $Zn_{1-x}Mn_xGeAs_2$ were grown from a stoichiometric ratio of high purity powders of $ZnAs_2$, Ge, and Mn, using the direct fusion method. The chemical composition was within the interval $0 \leq x \leq 0.078$. The technology of sample preparation is explained in detail in Ref. [13].

The preliminary studies of characteristics of $Zn_{1-x}Mn_xGeAs_2$ samples were undertaken and the results were presented in Refs. [2,14,15]. Using the X-ray diffraction spectra of powdered samples it was found that samples contain two main phases. These are solid solutions of Mn in $ZnGeAs_2$ and in $Zn_2Ge_{11}As_4$ compound, with chalcopyrite and zinc-blade cubic crystal structure, respectively. The magnetic properties of the alloy depend on the presence of Mn in the composition. Low Mn content produces a paramagnetic material, whereas larger amounts of Mn cause a ferromagnetic alignment of the alloy. From the results of the Hall measurements given in Table 1 it can be observed that the samples with relatively high density of the *p*-type free carrier, i.e. samples with $x = 0$, 0.013, and 0.047, have rather low mobility, whereas high mobility is associated with low density of the free carrier in samples with $x = 0.0028$, 0.053, and 0.078.

The presence of MnAs clusters in our $Zn_{1-x}Mn_xGeAs_2$ crystals was done with the use of a scanning electron microscope (SEM) coupled with energy dispersive x-ray spectrometer system (EDX). We used the field emission Hitachi SU-70 Analytical UHR FE-SEM SEM equipped with Thermo Scientific NSS 312 EDX system equipped with silicon drift detector. The samples surface was prepared prior to the SEM measurements including was mechanical polishing and chemical cleaning. The purpose of the sample preparation was to reduce the surface roughness and remove unintentional dirt and impurities. Our equipment allowed simultaneous use of the SEM and EDX techniques which in turn enabled to obtain images of the sample surface and the measurements of the localized elemental information at selected surface spots. A series of SEM maps was obtained for the $Zn_{1-x}Mn_xGeAs_2$ samples with different chemical composition. In agreement with our previous results [2] the SEM data showed no clustering for the samples with $x < 0.07$. For $x = 0.078$ the presence of MnAs clusters was observed (see Fig. 1).

The EDX results indicate the presence of MnAs clusters with diameter of about 10 μm. The stoichiometry of the $ZnGeAs_2$ equals 1:1:2 and the chemical content of MnAs inclusions is also close to 1:1.

The study of the CP2PM in *p*-type $Zn_{1-x}Mn_xGeAs_2$ was performed by measuring the far-infrared (FIR) reflection spectra at room temperature in the spectral range of 80 cm^{-1}–500 cm^{-1}, using BOMEM DA 8 spectrometer.

Table 1
Results of Hall measurements for $Zn_{1-x}Mn_xGeAs_2$.

x(Mn)	0	0.0028	0.013	0.047	0.053	0.078
p(10^{19} cm^{-3})	8.1	1.9	10.5	10.2	3.3	5.2
μ(cm^2/Vs)	19.1	67.8	14.9	15.3	44.1	28.7

3. Results and analysis

The far-infrared reflection spectra of single crystal samples of $Zn_{1-x}Mn_xGeAs_2$ are shown in Fig. 2. Each experimentally obtained data point is marked with a circular symbol. Two different spectra types are clearly visible. The samples with low free carrier density, i.e., samples corresponding to $x = 0.0028$, 0.053, and 0.078, show significant phonon structure. For the sample with $x = 0.0028$ the following features are distinguishable: the two dominant structures, clearly separated and located one in section 235 cm^{-1}–245 cm^{-1} and the other in 270 cm^{-1}–290 cm^{-1}, two phonons at about 210 cm^{-1} and 260 cm^{-1}, as well as the weakly expressed structures at approximately 120 cm^{-1} and 190 cm^{-1}. Note that stabilization of tetragonal structures occurred in this sample, according to the results of the X-ray measurements. The described features are visible in the spectra corresponding to $x = 0.053$ and $x = 0.078$, as well, however, in much less pronounced form. In these two cases it would be more appropriate to state that only the two most dominant structures are clearly visible.

When the free carrier density increases, i.e., for the samples corresponding to the remaining three values of *x*, the spectra take a completely different shape. Only the outlines of formerly clear structures can now be distinguished within a single wide shape, which should rather be described as a structure of slightly wavy shape. The most pronounced spectra from this group corresponds to $x = 0.047$. The phonon located at about 210 cm^{-1} and the structure positioned between 235 cm^{-1} and 245 cm^{-1} are broadened, merged, and spread up to 270 cm^{-1}, which is the lower limit of the most pronounced structure in previously described spectra and is now practically hidden by the electrons. The most pronounced became the structures located at about 180 cm^{-1} and 260 cm^{-1}, as well as the phonon positioned at approximately 90 cm^{-1}. The global minimum is shifted to above 320 cm^{-1}. Compared to the samples with low free carrier density, a noticeable reflectivity increase is registered in this area, as well.

A theoretical model of the bulk dielectric function has been discussed by several authors [6,16]. The low-frequency dielectric properties of single crystals are described by classical oscillators corresponding to the TO-modes, to which the Drude part is superimposed to take into account the free carrier contribution:

$$\varepsilon_S(\omega) = \varepsilon_\infty + \sum_{k=1}^{l} \frac{\varepsilon_\infty\left(\omega_{LOk}^2 - \omega_{TOk}^2\right)}{\omega_{TOk}^2 - \omega^2 - i\gamma_{TOk}\omega} - \frac{\varepsilon_\infty\omega_P^2}{\omega(\omega + i\Gamma_P)}, \quad (1)$$

where ε_∞ is the bound charge contribution and it is assumed to be a constant, ω_{LOk} and ω_{TOk} are the longitudinal and transverse optical-phonon frequencies, ω_P the plasma frequency, γ_{LOk} and γ_{TOk} indicate the damping of uncoupled modes of the host crystal, and Γ_P is the plasmon mode damping coefficient.

Our previous works [17–19] support the opinion that the structures located in the regions 235 cm^{-1}–245 cm^{-1} and 270 cm^{-1}–290 cm^{-1}, are a consequence of the combined plasmon-LO phonon modes, ω_{lj}. Therefore, we consider these two structures as good candidates for verification of CP2PM. The outcomes of the coupling between a single phonon and a plasmon, CPPM, for the various values of plasma damping Γ, are given in Fig. 3. The phonon is taken to be the E^2 phonon in $Zn_{1-x}Mn_xGeAs_2$, which in Eq. (1) corresponds to $l = 1$, $\omega_{TO} = 268$ cm^{-1}, and $\omega_{LO} = 273$ cm^{-1}, whereas ω_P defines the plasmon. The positions of the coupled mode were obtained from the real part of Eq. (1) as the solution of the equation $\mathrm{Re}\{\varepsilon_S\} = 0$ for $l = 1$. The obtained result is in excellent agreement with the GaAs case described in Ref. [5]. Further, each of the two structures taken as an example can be explained using the approach illustrated in Fig. 3, i.e., for the both cases the appropriate

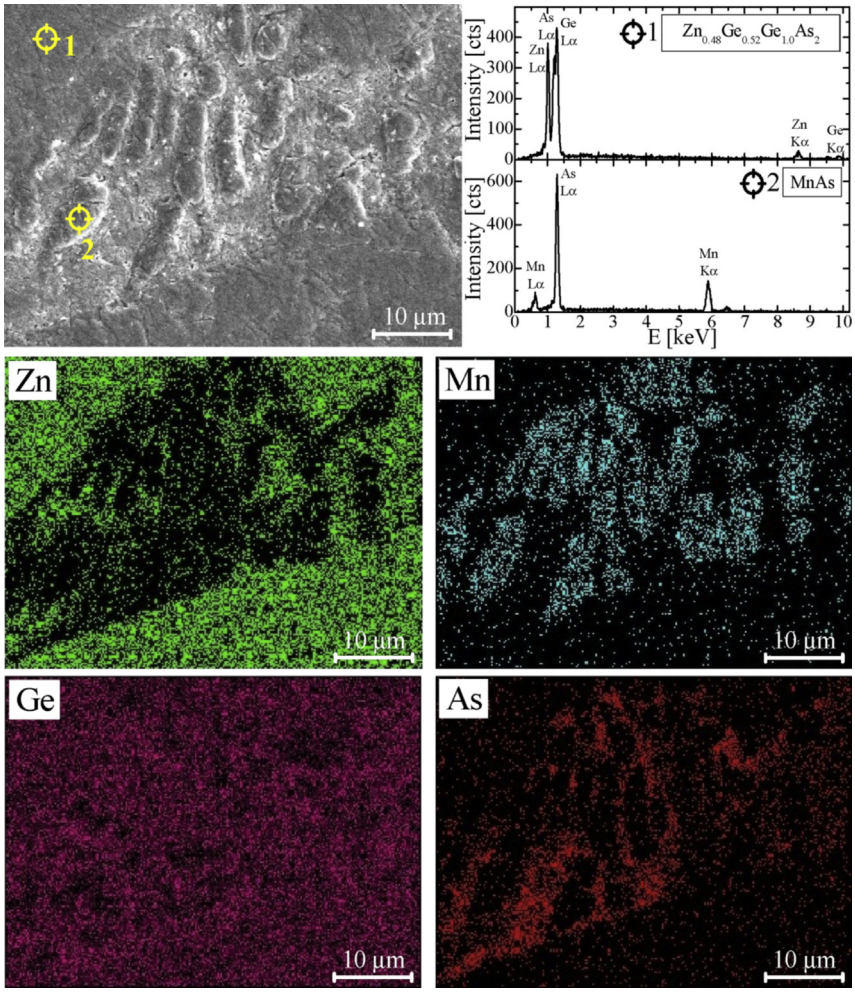

Fig. 1. Exemplary SEM image (top left) and EDX microprobe results including the detailed chemical content measurement (top right) and the maps of the distribution of the alloying elements obtained for the $Zn_{1-x}Mn_xGeAs_2$ sample with $x = 0.078$.

values of plasma frequency and damping can be determined to provide full description of the given structure. However, the dielectric function formed in such a way to account for the interaction of each individual phonon with the plasma, would lead to difficulties in understanding the nature of the multicomponent plasma. Several studies are dedicated to this issue [7–11].

With the intention to avoid the discussed difficulties and to establish better model of reflectivity spectra of $Zn_{1-x}Mn_xGeAs_2$, we used the dielectric function that includes in its initial form the interaction between two different LO phonons and a plasmon, i.e., the plasmon-two-phonons interaction [8,11], namely:

$$\varepsilon(\omega)=\varepsilon_\infty\frac{\prod_{j=1}^{3}\left(\omega^2+i\gamma_{lj}\omega-\omega_{lj}^2\right)}{\omega(\omega+i\Gamma_P)\prod_{i=1}^{2}\left(\omega^2+i\gamma_{ti}\omega-\omega_{ti}^2\right)}\times\prod_{k=1}^{s}\frac{\omega^2+i\gamma_{LOk}\omega-\omega_{LOk}^2}{\omega^2+i\gamma_{TOk}\omega-\omega_{TOk}^2}. \quad (2)$$

The first term in Eq. (2) represents coupling of a plasmon and two phonons, whereas the second term accounts for all s uncoupled modes of the crystal. The parameters ω_{lj} and γ_{lj} in the numerator of the first part are eigenfrequencies and damping coefficients of the longitudinal (LO) component of the plasmon-two-phonons waves, respectively. The parameters ω_{tj} and γ_{tj} in the denominator of the first part correspond to the corresponding characteristics of the transverse (TO) vibrations. The second factor represents uncoupled crystal modes, where ω_{LOk} and ω_{TOk} are the longitudinal and transverse frequencies, while γ_{LOk} and γ_{TOk} are the damping coefficients of the k-th crystal mode.

The dielectric function given with Eq. (2) was used to obtain the theoretical prediction of the experimental spectra shown in Fig. 2. The agreement between the experimental data shown as circles and the theoretical spectra given as solid lines is excellent.

The number of uncoupled phonons, s, depends on the manganese concentration, x, and will be discussed latter. In order to better understand the obtained results, the influence of the plasma damping on the positions of coupled plasmon-two-phonons modes is shown in Fig. 4. As explained earlier, the coupled mode positions are defined as the solutions of the real part of Eq. (1), i.e., $\mathrm{Re}\{\varepsilon_S\} = 0$; however, now under the condition $l = 2$.

The values of frequencies ω_{TO1} and ω_{TO2}, obtained as the best fit to experimental data, are 236 cm^{-1} and 268 cm^{-1} for E^3 and E^2, respectively. Ten values of the parameter Γ were considered, namely $\Gamma = 0$, 40, 60, 80, 100, 120, 140, 160, 180, and 250 cm^{-1}. The obtained dependence of the coupled modes positions depicted in Fig. 4 is qualitatively different from the one given in Fig. 3, which is expected since the number of coupled modes is different. For $\Gamma = 0$,

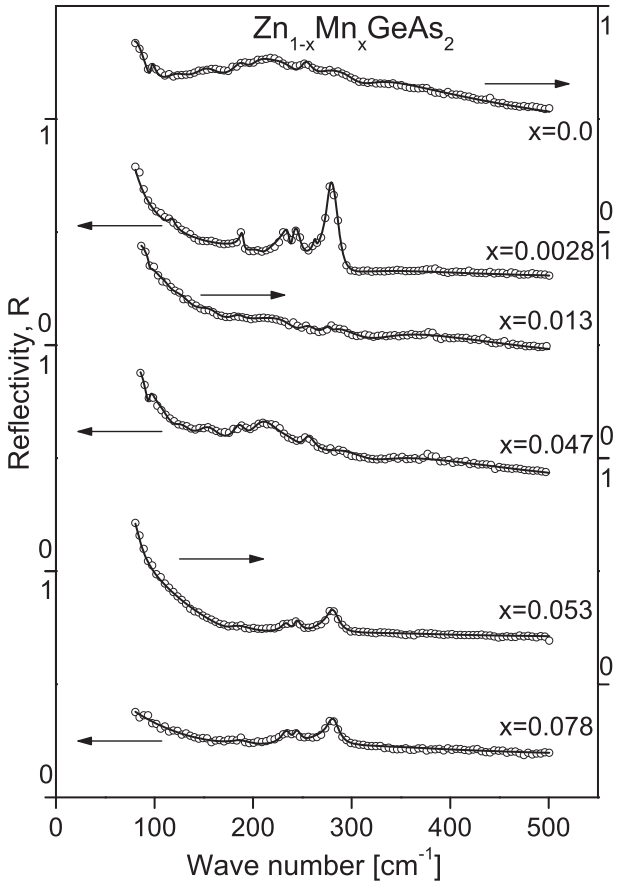

Fig. 2. Far-infrared reflection spectra of $Zn_{1-x}Mn_xGeAs_2$ single crystals. The experimentally obtained data points are depicted by circles. The theoretical spectra obtained with the model defined by Eq. (2) and fitting procedure are given as solid lines. Six different samples were considered with six values of manganese concentration $x = 0$, 0.0028, 0.013, 0.047, 0.053, and 0.078.

here as well as in Fig. 3, the lower branch starts as a plasmon and ends in TO1 phonons, whereas the upper branch begins as a phonon and ends in plasmon tail. The new branch, absent in Fig. 3, begins as LO1 phonon and approaches TO2 phonon at high values

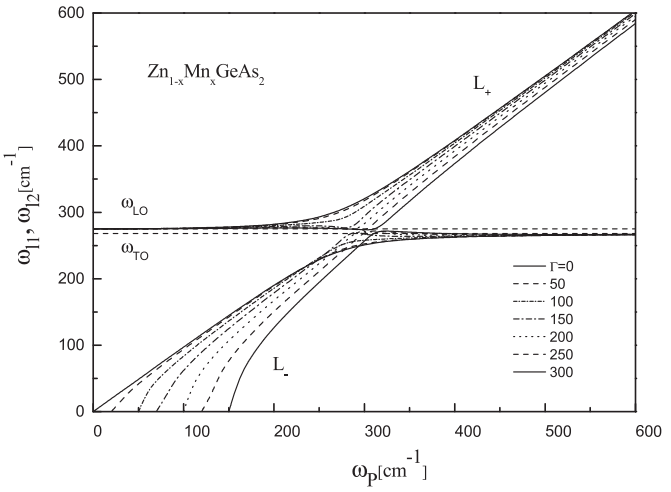

Fig. 3. Eigenfrequencies of plasmon–phonon modes for single crystal $Zn_{1-x}Mn_xGeAs_2$. The solid lines are spectra calculated from $Re\{\varepsilon_S\} = 0$, where ε_S is given by Eq. (1) whose parameter l is set to 1. Seven different values of plasma damping were considered, i.e., $\Gamma = 0$, 50, 100, 150, 200, 250, and 300 cm^{-1}.

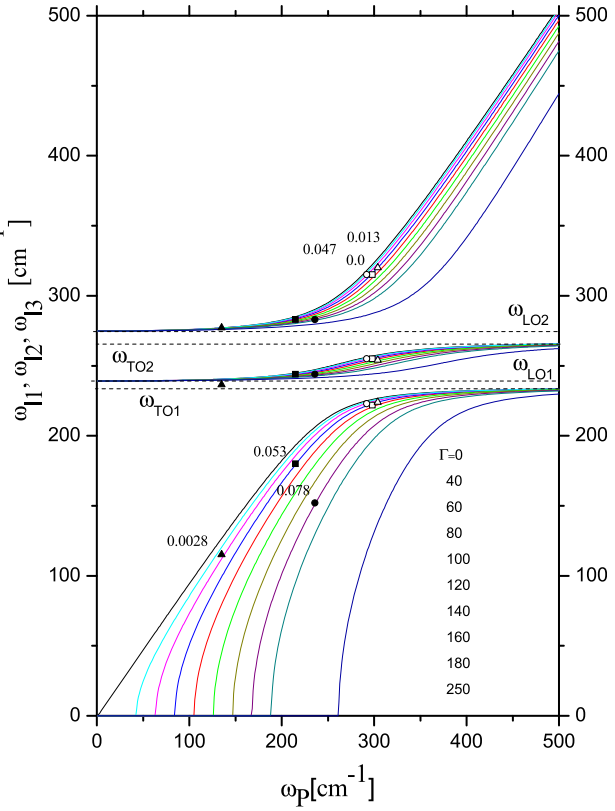

Fig. 4. Eigenfrequencies of plasmon-two-phonon modes for single crystal $Zn_{1-x}Mn_xGeAs_2$. The solid lines are spectra calculated from $Re\{\varepsilon_S\} = 0$, where ε_S is given by Eq. (1) whose parameter l is set to 2. Ten different values of plasma damping were considered, i.e., $\Gamma = 0$, 40, 60, 80, 100, 120, 140, 160, 180, and 250 cm^{-1}. Values obtained with Eq. (2) as the best fit to the experimental data in Fig. 1 are represented by solid symbols for samples with low free carrier density and open symbols for high free carrier density.

of plasma frequency. The values of LO phonon frequencies are obtained from Fig. 4 as a results of best fit. The nature of the branches does not change with the increase of plasma damping up to relatively large value of $\Gamma = 250$ cm^{-1}; instead, each branch is shifted within its range. The regions between TO1 and LO1, as well as between TO2 and LO2 are branch-free, as was the case with the TO–LO region in Fig. 3 for the LO phonon-plasmon interaction.

Results obtained as the best fit to the experimental data are in Fig. 4 denoted by different symbols for different values of x. The obtained values of plasma frequencies follow the change in free carrier density, N, which was expected since ω_P^2 is proportional to N. The most pronounced spectrum from each of the two groups, i.e., the one with $x = 0.0028$ and $x = 0.047$, correspond to the smallest value of plasma damping within its group.

There are three groups of uncoupled phonons. The first group contains the phonons that originated from $ZnGeAs_2$ and were detected in all spectra. These are the phonons located at around 101 cm^{-1}, 117 cm^{-1}, 161 cm^{-1}, and 210 cm^{-1}, with the B^3_1, E^5, E^4, and A_1 symmetry, respectively, as well as the group of phonons in the vicinity of 275 cm^{-1} whose symmetry is of the E^1 and B^1_2 type. These phonons are described in detail in Ref. [20].

The weak phonons around 180 cm^{-1} for $x = 0.053$ and 0.078, and above 320 cm^{-1} for $x = 0.013$ and 0.047, probably correspond to another detected phase, i.e., to $Zn_2Ge_{11}As_4$, or to the surface modes.

The most interesting is the third group of phonons at about 170 cm^{-1} which correspond to $x = 0.013$ and 0.047. Although their presence was noticeable in these two spectra, we did not observe

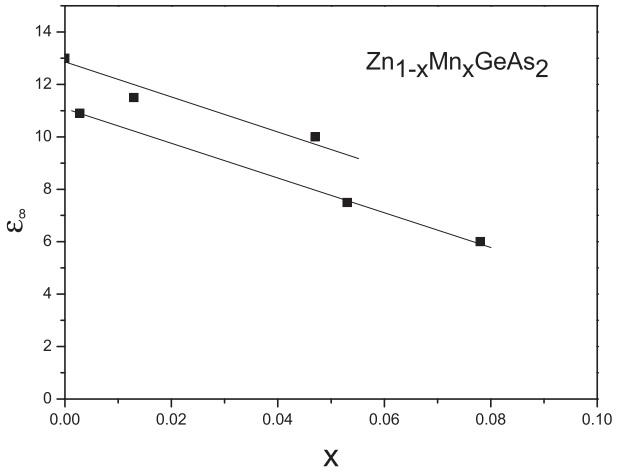

Fig. 5. Dependence of ε_∞ on manganese concentration.

these phonons in the spectra of the basic material. The calculated values of the MnAs clusters are positioned at these frequencies, as well [19]. Note that the Raman spectra measurements offer much more distinguished results. On the other hand, given the number of clusters and high free carrier density, for IR spectra it can be concluded with certainty only that it would not be possible to completely reproduce the spectra if these phonons were not taken into account.

The dependence of ε_∞ on the concentration of Mn is given quantitatively in Fig. 5. It was clear from Fig. 1 that ε_∞ decreases with the increase in Mn concentration. In addition to confirming this conclusion numerically, Fig. 5 shows that the dependence is linear within each of the two groups of samples that were established with respect to the free carrier density, i.e. for the group of samples with high as well as with low carrier density. The carrier density does not influence the shape of the dependence, i.e., the linearity; however, the group of samples with high carrier density has larger ε_∞ compared to the group with low carrier density.

4. Conclusion

We used far-infrared reflectivity measurements to investigate the influence of plasma damping on the interaction between a plasmon and two different phonons in $Zn_{1-x}Mn_xGeAs_2$. The specific nature of the behavior of the coupled phonons frequency is determined. At high plasma damping values entrance of phonons into the region between TO and LO frequencies is not observed for the plasmon-two-phonons interaction, unlike was the case with the plasmon-phonon interaction. Existence of MnAs clusters is confirmed and relation between free carrier concentration and optical parameters is determined.

Acknowledgments

This work was supported under the Agreement of Scientific Collaboration between Polish Academy of Science and Serbian Academy of Sciences and Arts. The work in Serbia was supported by the Serbian Ministry of Education, Science and Technological Development through Project 45003, and in Poland by National Science Center under granted decision No. DEC-2011/01/B/ST5/06602.

References

[1] S. Choi, G.B. Cha, S.C. Hong, S. Cho, Y. Kim, J.B. Ketterson, S.Y. Jeong, G.C. Yi, Solid State Commun. 122 (2002) 165.
[2] L. Kilanski, M. Gorska, W. Dobrowolski, E. Dynowska, M. Wojcik, B.J. Kowalski, J.R. Anderson, C.R. Rotundu, D.K. Maude, S.S. Varnavskiy, I.V. Fedorchenko, S.F. Marenkin, J. Appl. Phys. 108 (2010) 073925.
[3] W. Dobrowolski, J. Kossut, T. Story, Handbook of Magnetic Materials, Elsevier, Amsterdam, 2002.
[4] S. Picozzi, Nat. Mater 3 (2004) 349.
[5] G. Irmer, M. Wenzel, J. Monecke, Phys. Rev. B 56 (15) (1997) 9524.
[6] G. Abstreiter, M. Cardona, A. Pinczuk, in: M. Cardona, G. Guntherodt (Eds.), Light Scattering in Solids, IV, Springer-Verlag, Berlin, 1984.
[7] R.T. Holm, J.W. Gibson, E.D. Palik, J. Appl. Phys. 48 (1977) 212.
[8] A.A. Kukharski, Solid State Commun. 8 (1970) 1275.
[9] J. Trajić, N. Romčević, M. Romčević, V.N. Nikiforov, Mater. Res. Bull. 42 (2007) 2192–2201.
[10] J. Trajić, N. Romčević, M. Romčević, D. Stojanović, R. Rudolf, T.A. Kuznetsova, D.R. Khokhlov, J. Alloys Compd. 493 (2010) 41–46.
[11] M. Petrovic, N. Romcevic, J. Trajic, W.D. Dobrowolski, M. Romcevic, B. Hadzic, M. Gilic, A. Mycelski, Infrared Phys. Technol. 87 (2014) 323–326.
[12] M. Romčević, N. Romčević, W. Dobrowolski, L. Kalinski, J. Trajić, D.V. Timotijević, E. Dynowska, I.V. Fedorchenko, S.F. Marenkin, J. Alloys Compd. 548 (2013) 33–37.
[13] V.M. Novotortsev, V.T. Kalinnikov, L.I. Koroleva, R.V. Demin, S.F. Marenkin, T.G. Aminov, G.G. Shabunina, S.V. Boichuk, V.A. Ivanov, Russ. J. Inorg. Chem. 50 (2005) 429.
[14] V.M. Novovotortsev, S.F. Marenkin, S.A. Varnavskii, L.I. Koroleva, T.A. Kupriyanova, R. Szymcak, L. Kilanski, B. Krzmanska, Russi. J. Inorg. Chem. 53 (2008) 22.
[15] L.I. Koroleva, V.Yu Pavlov, D.M. Zashhchirinskii, S.F. Marenkin, S.A. Varnavskii, R. Szimczak, W. Dobrowolski, L. Kilanski, Phys. Solid Sate 49 (2007) 2121.
[16] E. Burstein, A. Pinczuk, R.F. Wallis, in: D.L. Carter, R.T. Bate (Eds.), The Phys. Of Semimetals and Narrow-Gap Semicon, 1971. Pergamon, New York.
[17] M. Romcevic, L. Kilanski, N. Romcevic, B. Hadzic, W. Dobrowolski, I.V. Fedorchenko, S.F. Marenkin, Mater. Res. Bull. 59 (2014) 300–304.
[18] J. Trajić, N. Romčević, M. Romčević, D. Stojanović, L.I. Ryabova, D.R. Khokhlov, J. Alloys Compd. 602 (2014) 300–305.
[19] N. Romčević, J. Trajić, T.A. Kuznetsova, M. Romčević, B. Hadžić, D.R. Khokhlov, J. Alloys Compd. 442 (2007) 324–327.
[20] F.W. Ohrendorf, H. Haeuseler, Cryst. Res. Technol. 34 (1999) 339–349.